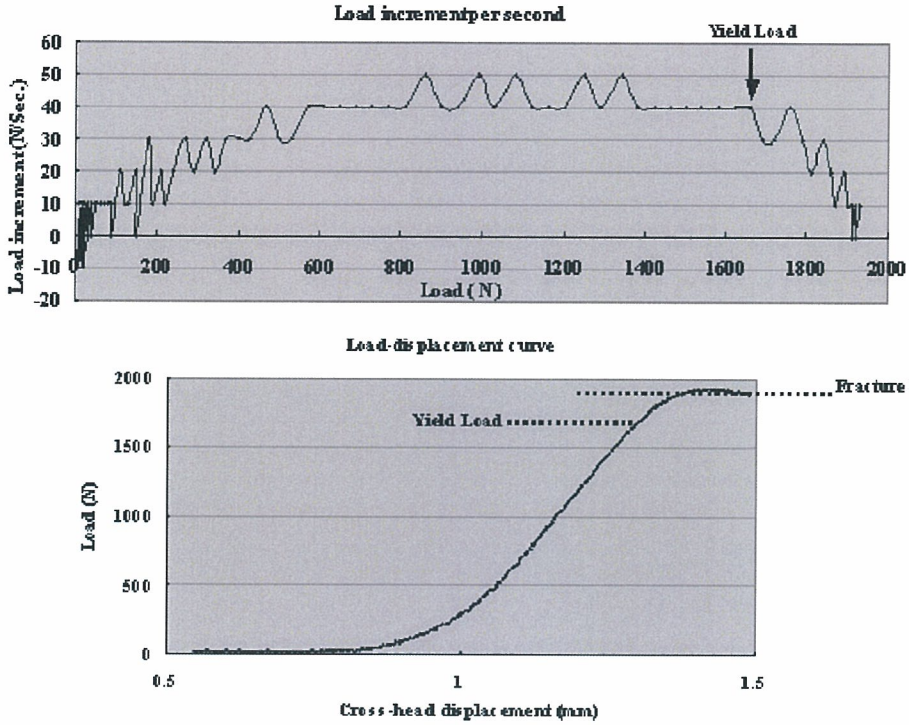

Figure 2. The definition of the experimental yield load and the fracture load. The experimentally measured yield load was defined as the load that reached the end of the constant load increment rate. The measured fracture load was defined as the ultimate load achieved.

Results

There was a significant linear correlation between the yield loads predicted by the FE analysis and those of the measured ($r = 0.949$, $P < 0.0001$) (Figure 4). The correlation between the FE predicted fracture loads and the measured was even stronger ($r = 0.978$, $P < 0.0001$), and the slope of the regression line was 0.8807 (Figure 5). There was also a significant linear correlation between the FE predicted minimum principal strain and the measured ($r = 0.838$, $P < 0.0001$) (Figure 6).

There were two types of experimental fractures. Obvious fracture lines were recognized in six vertebrae. There were no obvious fracture lines in the other six, but they had apparent residual deformities after the mechanical testing. The anterior part of the vertebra was compressed in three of the six. The other two sustained middle part compression and in one there was compression of the entire vertebra.

The experimental fracture line in the specimen was found to pass through a region of the failed elements on the simulation model (Figure 7). In addition, the FE analysis of the minimum principal strain at the midsagittal section disclosed that the area with a large absolute value of this predicted minimum principal strain agreed well with the experimental fracture site and that it visualized the fractured area.

In the specimens with anterior compression, marked radiolucency was recognized at the anterior part of the

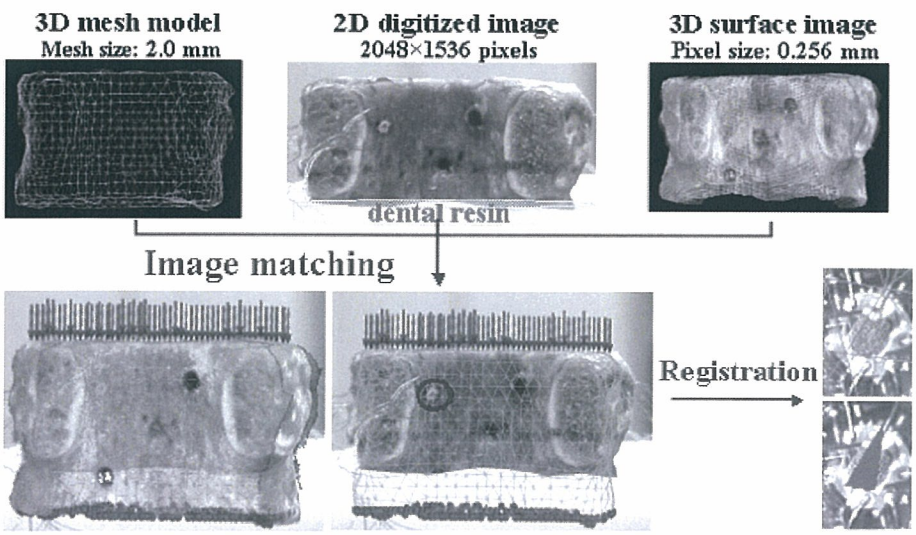

Figure 3. A three-dimensional surface acquisition system was employed to identify the gauge attachment sites by matching the three-dimensional surface image with the FE model. The three-dimensional mesh model, the two-dimensional digitized image, and the three-dimensional surface image, were matched and the strain gauge attachment sites were then identified.

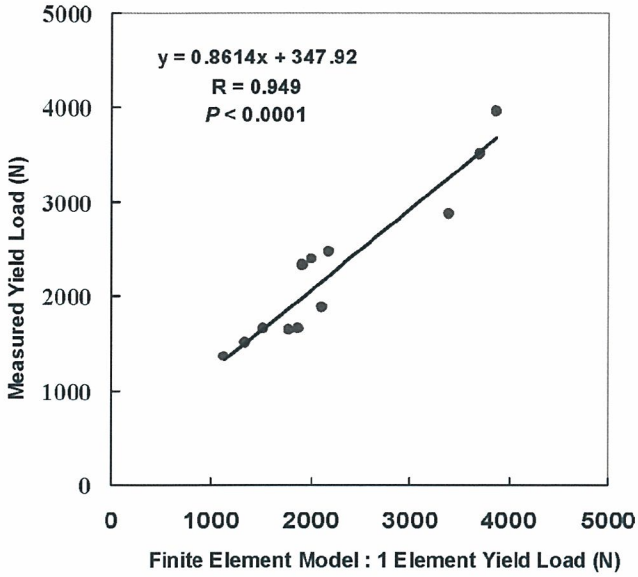

Figure 4. The experimentally measured yield loads versus the yield loads predicted by the finite element (FE) analysis. They were significantly correlated.

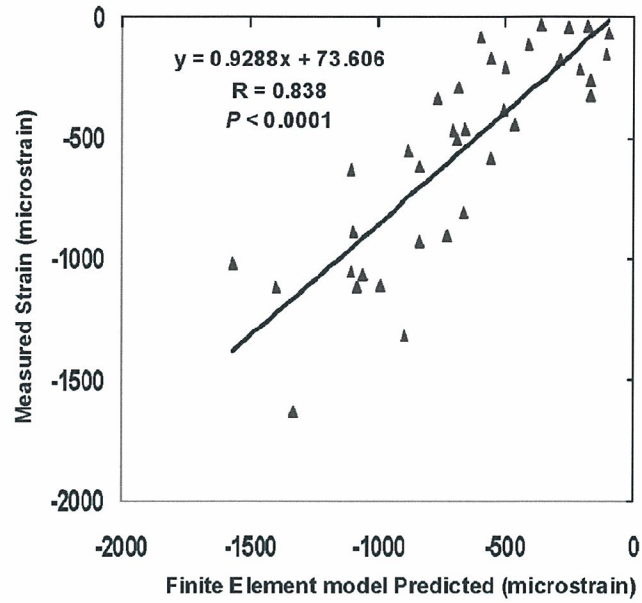

Figure 6. The values of measured minimum principal strain versus those of minimum principal strain predicted by the FE model. Significant correlation was also obtained.

vertebra, where the trabecular pattern was observed to be very coarse (Figure 8). The FE analysis showed that the failed elements appeared at the same anterior part as the area with coarse trabeculae. Likewise, the area with large absolute value of the minimum principal strain localized at the anterior part, which agreed with the area of the experimental compression fracture.

Discussion

The correlations between the measured values of fracture strength and the predicted values with the FE model were very good (r = 0.978) and better than the previous FE studies (r = 0.89–0.95). The characteristics of the FE model in this study were as follows: adoption of tetrahedron elements to precisely model surface curvatures of the entire vertebra, utilization of nonlinear analysis to match the elastoplasticity of the vertebra in compression, construction of cortical shells on the surface of the model, and adoption of Drucker-Prager equivalent stress instead of von Mises stress as a criterion of an element yield. Which of these factors contributed most to the results was not determined in this study because we did not separate these characteristics to analyze each factor's contribution. Clarification of this feature will be one of our targets for the next study.

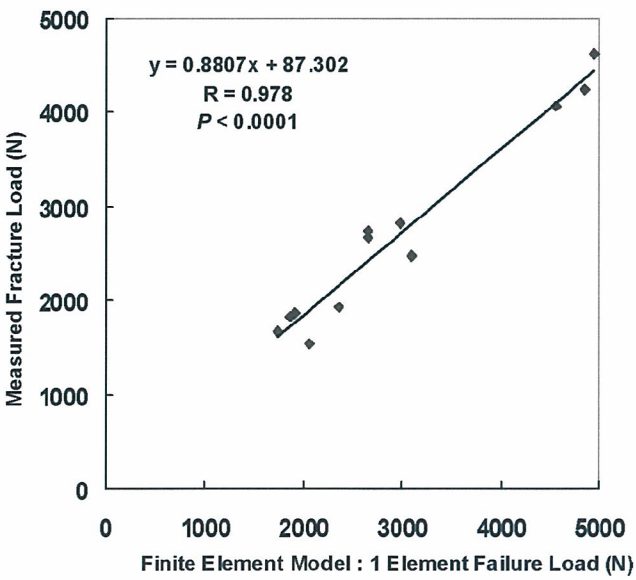

Figure 5. The measured fracture loads versus the fracture loads predicted by the FE model. The correlation was much better with a slope of 0.8807.

With tetrahedron elements, it was possible to create a more proximate, realistic and smooth surface contour than with hexahedral elements, which could possibly avoid any artificial stress raisers.

With the currently available CT resolution, strength of the cortical shell tended to be underestimated. In CT-based FE models, density of this shell has been underestimated because it is dependent on its Hounsfield unit value. It has been reported that in previous experiments thin cortical shell of the vertebrae contributed approximately 10% to the overall vertebral strength in healthy individuals and the contribution of the cortical shell was estimated to be significantly larger in osteoporotic individuals.[2,30] Thus, the importance of the strength of the cortical shell should be taken into consideration in predicting the fracture load of osteoporotic individuals.

Overaker *et al* set the thickness of the anterior cortex as 0.6 mm and that of the posterior as 0.4 mm; they set the cortical Young's modulus as 5, 6, 7 GPa. They concluded that Young's modulus of 7 GPa precisely correlated with the experimental result.[29] Liebschner *et al* set the thickness as 0.35 mm and Young's modulus as 0.475 GPa.[15] We

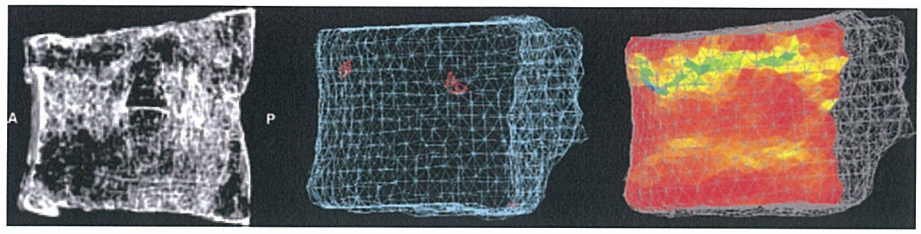

Figure 7. The reconstructed micro-CT images (A, anterior; P, posterior), the failed elements, and the minimum principal strain distribution at the mid-section analyzed by the FE model. The failed elements appeared right on the actual fracture line. The minimum principal strain distribution agreed well with the experimental fracture line.

constructed a cortical shell with a thickness of 0.4 mm and Young's modulus of 10 GPa. The cortical area with a thickness of more than 0.4 mm was modeled with both the shell and the tetrahedron element adjacent to the shell.

Young's modulus of human cortical bone has been reported to be 15 GPa,[31] 19.9 GPa (dynamic), and 16.2 GPa (static).[32] Young's modulus of human vertebra cancellous tissue was reported as 3.8 to 13.4 GPa,[25–28] but few data of cortical shell have been available. Thus, it was necessary to set our own value. Young's modulus of the cortical shell obtained from the QCT data were 7 GPa. QCT underestimated the cortical shell density, so the actual density was estimated to be higher than that derived from QCT. Therefore, we set Young's modulus as 10 GPa, and then the values of the minimum principal strain were accurately predicted with a correlation coefficient of 0.838 and a slope of the regression line of 0.9288.

In previous studies, von Mises equivalent stress has been used as the criterion of yield.[8,10,13] For ductile materials such as metals, von Mises criterion would be effective, but for bones it seems more appropriate to use Drucker-Prager equivalent stress. The yield strain of human vertebral trabecular bone was reported −7,000 to −10,000 microstrain.[17,18] Therefore, we adopted minimum strain of −10,000 microstrain as a criterion for element collapse.

Some previous reports described the mechanical properties of human bone. We tested three theories: Carter and Hayes' property,[33,34] Keller's,[35] and Keyak's.[10] With Carter and Hayes' property, the predicted fracture loads were about 60% and using Keller's, the predicted fracture loads were about 120% of those of the experiment. Accurate prediction could be made with Keyak's, although further investigations will be necessary to obtain the actual mechanical properties of human vertebra.

In this investigation, prediction of the ultimate load was more accurate than that of the yield load. One possibility was that determination of the experimental yield load was not appropriate. The ultimate load was clearly determined, but the yield load was objectively determined from load *versus* displacement curves by calculating the load increment rate (Figure 2).

There were two types of vertebral fracture: one showed fracture line and the other showed no fracture lines but had apparent residual deformities. Both fracture types could be predicted. Fracture location was most accurately predicted by the distribution of very low levels of the minimum principal strain. Therefore, we speculated that fracture was initiated at the sites of failed elements and propagated along with the area with very low minimum principal strain.

The prediction was made under a very simple loading condition with quasi-static uniaxial vertical loading. The condition was the simplest, but it minimized experimental error, which might have occurred to some degree with complicated loading conditions. Arbitrary load magnitude or direction can be set for the same simulation model. So it is possible to analyze strength or fracture site of vertebrae for loading conditions that actually cause fractures, although it would be very hard to create these fractures under an experimental condition. To predict in vivo behavior of spinal bones is another target for our next study.

To verify our model, we evaluated three factors: fracture strength, fracture site, and strain on the surface of the vertebrae. Prediction of only fracture strength would not be adequate to evaluate the accuracy of FE analysis. Predicted fracture sites should also be matched with those of the experiment, and the process by which deformation of the vertebrae proceeds should be simulated. To attain this, we used strain gauges to measure surface strain throughout the loading process. This has not been done in previous studies investigating the accuracy of a simulation model.

The limitation is the cortical shell was treated as a homogeneous material because the pixel spacing with

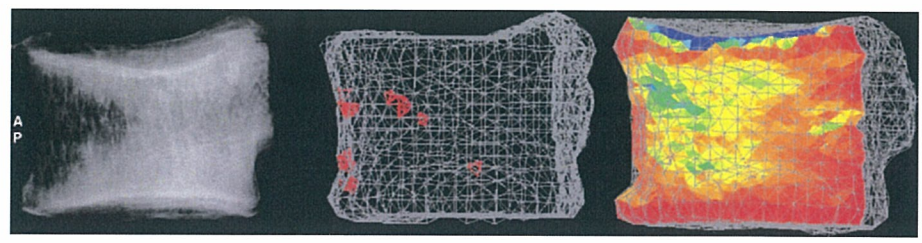

Figure 8. Radiogram after the mechanical testing, showing sparse trabecula in the anterior part of the vertebral body. The failed elements agreed well with the site of the experimental fracture. The minimum principal strain distribution also agreed well with the area of the experimental fracture.

CT is too large to model the thin cortical shell. If a CT with improved resolution becomes available, it would make it possible to model the cortical shell with heterogeneous properties, thus enabling creation of a more realistic model.

There is another limitation. The posterior portion of the vertebra was excised in this study. A three-dimensional surface acquisition system using an image encoder was used to identify the gauge attachment sites on the shell elements. With the posterior portion of the vertebra such as lamina or spinous process, obtaining three-dimensional surface image of the posterior part of the vertebral body should be interfered. It was one of the reasons why the posterior portion of the vertebra was excised. Clinically, most of the vertebral fractures occur at the vertebral body. However, the posterior portion of the vertebra might share some ratio of axial loading. Therefore, loading environment in the in vivo situation may be different from that in this study. To predict in vivo behavior of spinal bones, the posterior portion of the vertebra must be included.

The cadaveric specimens were all extracted from males, whose bone quality might be somewhat different from that of females. To use this model as a diagnostic tool for osteoporosis, it would have been better to use specimens from both males and females. Validation of accurate prediction by the FE model in an experiment using female cadaveric specimens will be another target of our future study. Furthermore, true efficacy of this method will be validated after a large-scale cohort study investigating the association between the predicted fracture loads in the study groups and the occurrence rates of actual fracture in the same groups. It is expected that this method will be valuable in estimating fracture risk of vertebrae in osteoporotic individuals.

■ Key Points

- Vertebral strength and fracture site were accurately predicted using nonlinear finite element model.
- The minimum principal strain at the vertebral surface was also predicted.
- The experimental fracture sites corresponded with the sites where the elements were predicted to fail.

References

1. Mosekilde L, Bentzen SM, Ortoft G, et al. The predictive value of quantitative computed tomography for vertebral body compressive strength and ash density. *Bone* 1989;10:465–70.
2. McBroom RJ, Hayes WC, Edwards WT, et al. Prediction of vertebral body compressive fracture using quantitative computed tomography. *J Bone Joint Surg Am* 1985;67:1206–14.
3. Brinckmann P, Biggemann M, Hilweg D, et al. Prediction of the compressive strength of human lumbar vertebrae. *Clin Biomech* 1989;4(suppl):1–27.
4. Edmondston SJ, Singer KP, Day RE, et al. In-vitro relationships between vertebral body density, size and compressive strength in the elderly thoracolumbar spine. *Clin Biomech* 1994;9:180–6.
5. Cheng XG, Nicholson PH, Boonen S, et al. Prediction of vertebral strength in vitro by spinal bone densitometry and calcaneal ultrasound. *J Bone Miner Res* 1997;12:721–8.
6. Myers BS, Arbogast KB, Lobaugh B, et al. Improved assessment of lumbar vertebral body strength using supine lateral dual-energy x-ray absorptiometry. *J Bone Miner Res* 1994;9:687–93.
7. Bjarnason K, Hassager C, Svendsen OL, et al. Anteroposterior and lateral spinal DXA for the assessment of vertebral body strength: comparison with hip and forearm measurement. *Osteoporos Int* 1996;6:37–42.
8. Lotz JC, Cheal EJ, Hayes WC. Fracture prediction for the proximal femur using finite element models: I. Linear analysis. *J Biomech Eng* 1991;113:353–60.
9. Lotz JC, Cheal EJ, Hayes WC. Fracture prediction for the proximal femur using finite element models: II. Nonlinear analysis. *J Biomech Eng* 1991; 113:361–5.
10. Keyak JH, Rossi SA, Jones KA, et al. Prediction of femoral fracture load using automated finite element modeling. *J Biomech* 1998;31:125–33.
11. Keyak JH. Improved prediction of proximal femoral fracture load using nonlinear finite element models. *Med Eng Phys* 2001;23:165–73.
12. Cody DD, Gross GJ, Hou FJ, et al. Femoral strength is better predicted by finite element models than QCT and DXA. *J Biomech* 1999;32:1013–20.
13. Silva MJ, Keaveny TM, Hayes WC. Computed tomography-based finite element analysis predicts failure loads and fracture patterns for vertebral sections. *J Orthop Res* 1998;16:300–8.
14. Martin H, Werner J, Andresen R, et al. Noninvasive assessment of stiffness and failure load of human vertebrae from CT-data. *Biomed Tech* 1998;43:82–8.
15. Liebschner MA, Kopperdahl DL, Rosenberg WS, et al. Finite element modeling of the human thoracolumbar spine. *Spine* 2003;28:559–65.
16. Crawford RP, Cann CE, Keaveny TM. Finite element models predict in vitro vertebral body compressive strength better than quantitative computed tomography. *Bone* 2003;33:744–50.
17. Keaveny TM, Wachtel EF, Ford CM, et al. Differences between the tensile and compressive strengths of bovine tibial trabecular bone depend on modulus. *J Biomech* 1994;27:1137–46.
18. Kopperdahl DL, Keaveny TM. Yield strain behavior of trabecular bone. *J Biomech* 1998;31:601–8.
19. Morgan EF, Keaveny TM. Dependence of yield strain of human trabecular bone on anatomic site. *J Biomech* 2001;34:569–77.
20. Silva MJ, Wang C, Keaveny TM, et al. Direct and computed tomography thickness measurements of the human, lumbar vertebral shell and endplate. *Bone* 1994;15:409–14.
21. Vesterby A, Mosekilde L, Gundersen HJ, et al. Biologically meaningful determinants of the in vitro strength of lumbar vertebrae. *Bone* 1991;12: 219–24.
22. Mosekilde L. Vertebral structure and strength in vivo and in vitro. *Calcif Tissue Int* 1993;53(suppl):121–6.
23. Dougherty G, Newman D. Measurement of thickness and density of thin structures by computed tomography: a simulation study. *Med Phys* 1999; 26:1341–8.
24. Prevrhal S, Engelke K, Kalender WA. Accuracy limits for the determination of cortical width and density: the influence of object size and CT imaging parameters. *Phys Med Biol* 1999;44:751–64.
25. Jensen KS, Mosekilde L. A model of vertebral trabecular bone architecture and its mechanical properties. *Bone* 1990;11:417–23.
26. Rho JY, Tsui TY, Pharr GM. Elastic properties of human cortical and trabecular lamellar bone measured by nanoindentation. *Biomaterials* 1997; 18:1325–30.
27. Hou FJ, Lang SM, Hoshaw SJ, et al. Human vertebral body apparent and hard tissue stiffness. *J Biomech* 1998;31:1009–15.
28. Ladd AJ, Kinney JH, Haupt DL, et al. Finite-element modeling of trabecular bone: comparison with mechanical testing and determination of tissue modulus. *J Orthop Res* 1998;16:622–8.
29. Overaker DW, Langrana NA, Cuitino AM. Finite element analysis of vertebral body mechanics with a nonlinear microstructural model for the trabecular core. *J Biomech Eng* 1999;121:542–50.
30. Faulkner KG, Cann CE, Hasegawa BH. Effect of bone distribution on vertebral strength: assessment with patient-specific nonlinear finite element analysis. *Radiology* 1991;179:669–74.
31. Choi K, Kuhn JL, Ciarelli MJ, et al. The elastic moduli of human subchondral, trabecular, and cortical bone tissue and the size-dependency of cortical bone modulus. *J Biomech* 1990;23:1103–13.
32. Katsamanis F, Raftopoulos DD. Determination of mechanical properties of human femoral cortical bone by the Hopkinson bar stress technique. *J Biomech* 1990;23:1173–84.
33. Carter DR, Hayes WC. Bone compressive strength: the influence of density and strain rate. *Science* 1976;194:1174–6.
34. Carter DR, Hayes WC. The compressive behavior of bone as a two-phase porous structure. *J Bone Joint Surg Am* 1977;59:954–62.
35. Keller TS. Predicting the compressive mechanical behavior of bone. *J Biomech* 1994;27:1159–68.

Available online at www.sciencedirect.com
SCIENCE DIRECT®
Clinical Biomechanics 20 (2005) 421–427
CLINICAL BIOMECHANICS
www.elsevier.com/locate/clinbiomech

Measurement of the tensile forces during bone lengthening

Isao Ohnishi *, Takahide Kurokawa, Wakyo Sato, Kozo Nakamura

Faculty of Medicine, Department of Orthopaedic Surgery, University of Tokyo, 7-3-1 Hongo, Bunkyo-ku, Tokyo, 113-0033, Japan

Received 29 July 2004; accepted 25 October 2004

Abstract

Background. The purpose of this study was to investigate the effects of lengthening frequency on mechanical environment in limb lengthening.

Methods. Tensile forces were continuously monitored using a load sensor attached to a unilateral external fixator. Twenty patients were monitored. Ten patients were with acquired femoral shortening, and five of them underwent quasi-continuous lengthening of 1440 steps per day, and the other five received step lengthening twice a day. The other 10 patients were with achondropalsia. Five of them underwent the same quasi-continuous lengthening, and the other five received the same step lengthening. The circadian change and the daily course of the tensile forces were assessed and compared between quasi-continuous lengthening and step lengthening.

Findings. As for circadian change, an acute increase in the force took place simultaneously with each step of lengthening in the step-lengthening group, but very little change of the baseline force level was seen during quasi-continuous lengthening. As for daily course of the tensile force, it increased almost linearly in both lengthening frequency groups in the initial stage of lengthening. No significant difference of the average force increment rate in this phase was recognized between the quasi-continuous and step lengthening groups irrespective of the etiologies.

Interpretation. The lengthening frequency greatly affected the circadian change of the tensile force, but did not affect the increment rate of the force in the linear phase.

Keywords: Tensile force; Bone lengthening; Quasi-continuous lengthening; Automated lengthener; Load sensor

1. Introduction

A small increment of the distance between bone fragments is added daily after osteotomy and a week of waiting period in the callus distraction technique. As the inter-fragmental distance increases, tensile force is generated in the callus and soft tissues by distraction, and an equivalent amount of compressive force is applied on the bone fragments. Because of viscoelasticity of the soft tissues, the increase in the tensile force varies with parameters such as the increment, rate, and frequency of lengthening (Leong et al., 1979). An increase in the axial length of the soft tissues as a result of structural changes leads to a decrease in the tensile force. Thus, monitoring of this force can not only provide a way to control the rate or frequency of lengthening (van Roemund et al., 1992) and prevent the overstretching of soft tissues, but can also supply a method of detecting soft tissue structural changes in real time.

Serious complications may occur as the tensile force increases with lengthening. For example, overstretching of the soft tissues may cause pain or even nerve palsy (Galardi et al., 1990). In almost every case, we encounter the complication of contracture, and sometimes this is irreversible after lengthening has been accomplished. Bowing deformities of the lengthening bone may occur

* Corresponding author.
E-mail address: ohnishii-dis@h.u-tokyo.ac.jp (I. Ohnishi).

0268-0033/$ - see front matter © 2004 Elsevier Ltd. All rights reserved.
doi:10.1016/j.clinbiomech.2004.10.010

when the considerable compressive force or moment generated on the fragment end produces elastic or even plastic deformation of the pins or fixator body (Simpson et al., 1996). Elevation of the intra-articular pressure in joints adjacent to the lengthened bones may cause pathological changes of the articular cartilage. Hiroshima has reported three cases where narrowing of the joint space of the hip persisted after femoral lengthening (Hiroshima, 1992). Therefore, various unfavorable effects may arise due to an excessive increase in the soft tissue tensile force. Thus, control of this force and avoidance of its excessive elevation by continuous monitoring are thought to be desirable procedures to follow during lengthening (Matsushita et al., 1999). In addition, the rate and frequency of lengthening should be determined not only by estimating the amount of callus formation but also by taking this tensile force into consideration.

By performing continuous lengthening using an automated lengthener, it is possible to minimize the distraction distance per step by greatly increasing the frequency of the distraction steps. Whether such auto-continuous lengthening has some advantages over the usual lengthening method is still unknown, but monitoring of the tensile force could be an effective way to evaluate the influence of the automated method on the soft tissues.

The Hifixator (Nagano Keiki Co. Ltd., Ueda, Japan) is a unilateral external fixator composed of a titanium cylinder shaft and two pin clamps, which is equipped with a pressure sensor to monitor the load applied axially to the bone fragments. This study investigated the changes in tensile forces during both the quasi-continuous lengthening and the step lengthening to know the differences of reactive forces generated in the tissues under distraction.

2. Methods

First of all, an in vitro loading test with a bone model fixed with an external fixator was performed to evaluate accuracy of the measurement. The Hifixator is equipped with a dynamic pin clamp with a ball bearing mechanism which allows sooth sliding excursion along the shaft when loaded (Ohnishi et al., 2002). A force transducer was attached to the dynamic pin clamp and measured the axial load acted on the bone fragment fixed with the fixator (Fig. 1).

2.1. Accuracy assessment in the tensile force measurement

A bone model which was made of stainless steel rod with a diameter of 32 mm was fixed with a Hifixator via three pins with a diameter of 6 mm. The distance between the fixator and the bone model was set at 60 mm and 70 mm. The distance between the proximal and distal pin-clamps was set at 150 mm. The bone model was loaded axially with incremental increases and decreases of the load from 0 to 700 N. The force readings of the load cell of the testing machine (U3G1-500K, Shinko Engineering Co. Ltd., Gifu, Japan) were compared to those of the force transducer of the fixator. Linearity and hysteresis of these measurements were evaluated.

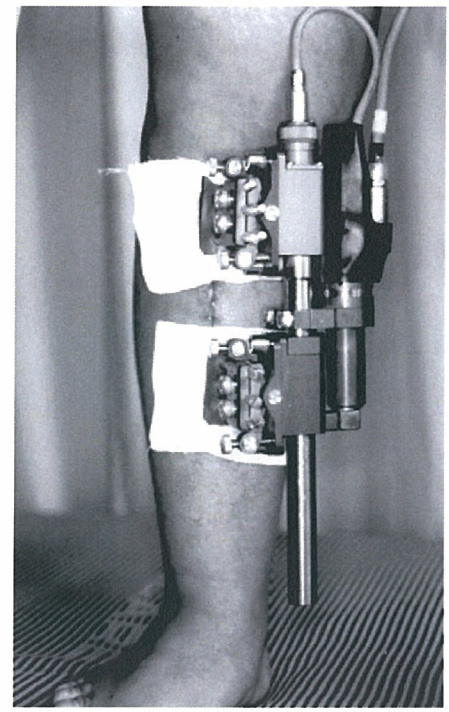

Fig. 1. A force transducer was attached to a dynamic pin clamp and measured the axial load acted on the bone fragment fixed with the fixator. An auto-lengthener is mounted on the fixator capable of quasi-continuous lengthening with 1440 steps per day.

2.2. Monitoring tensile forces in patients

Then, continuous 24-h monitoring of the tensile force was performed during limb lengthening using a Hifixator with a force transducer, and readings were automatically recorded at predetermined time intervals. Total of 20 male patients were studied. There were 10 patients with unilateral femoral shortening after previous fracture or infantile injury of the distal growth plate. The average shortening was 60 mm with a range of 35–85 mm. Another 10 patients were with short stature due to acondroplasia, all of whom underwent bilateral tibial lengthening. The average age at the time of lengthening was 19.8 years with a range of 15–37 years. All of the subjects were treated using the callus distraction technique after osteotomy at the proximal sub-metaphysis.

Five patients from each of the two groups who were randomly allocated and approved the informed consent underwent auto-continuous lengthening using an auto-

lengthener which acted at 1-min intervals. Therefore, the total amount of lengthening in one day was divided into 1440 times. The rate of lengthening was 0.3–1.0 μm/min (mean: 0.7 μm/min or 1.0 mm/day). The auto-lengthener was constructed with a driving unit and a controller which precisely regulated the amount of each lengthening at every extremely short interval. The driving unit was equipped with a driving pin, a DC motor, a deaccelerator and an encoder. The maximum driving force was 700 N with a proof driving force of 500 N. The maximum driving speed was 0.7 mm/min. The weight of the lengthener was 270 g. The number of the turns of the DC motor was detected by a photo encoder. The information on the previous number of the turns was transferred to an up–down counter of the encoder, and the signal of the encoder was processed by a micro-computer installed in the controller to calculate the amount of lengthening of the next step. The auto-lengthening system had several fail safe mechanisms. First, cables durable for bending were used to avoid disconnection. In case of failure of the encoder cable, the motor might have possibility to continue working. To avoid this situation, electricity consumption and the voltage were kept monitoring throughout operation. When abnormal values could be detected, the operation system was designed to switch off the motor. In addition, the motor current flow was programmed to automatically stop after 15 s. The controller shielded any abnormal current from outside. The other five patients in each group underwent the standard step lengthening procedure using the same fixator (0.5 mm or 0.25 mm at 12-h intervals; mean: 1.0 mm/day).

All procedures in the bone lengthening treatment protocol using an auto-lengthener were approved by the ethics committee in our institution. The treatment was also approved by each of the patients with informed consent.

A load sensor was attached to the first pin clamp coaxially with the shaft of the fixator and it measured the tensile force in unit of 1 N. The load sensor was very small with a diameter of 1.5 cm and was screwed into the pin clamp. The sensing equipment was composed of semiconductor strain gauges and a discoid diaphragm. Only the right side of the leg was monitored in patients with bilateral tibial lengthening. The monitoring of the load was commenced just after initiation of lengthening and kept until the final day of the lengthening.

After the signals of the load sensor were transferred to an amplifier, the readings were stored in a portable data recorder (DL100, Teac Co. Ltd., Tokyo, Japan). The measured values were analyzed with a personal computer and plotted using a graph plotter (YEW Model 3023, Yokogawa, Tokyo, Japan). By digital recording, continuous logging of the instantaneous load values was performed at 1-min intervals. A graph of the circadian change of the load was made by directly plotting the instantaneous data, while plotting the average load values at 15-min intervals made a graph of the daily course of the load. A part of the data was recorded with a chart recorder (YEW Model 305643).

Due to bending of the fixation pins under load generated during lengthening, acquired length was measured using a vernier caliper between the inner pins situated either side of, and close to the leg. In order to minimize angular deformity generated during lengthening, alignment of the bone fragment was repeatedly adjusted by rotating the pin clamps using a specially designed zig.

The circadian change of the baseline tensile force was evaluated and compared between the patients with quasi continuous lengthening and those with step lengthening for both etiologies. The daily course of the baseline tensile force was also assessed and compared between the patients with quasi continuous lengthening and those with step lengthening for both etiologies.

Increasing rates of the tensile forces was assessed during the initial linear phase of the load, and the increment rates of the tensile forces with a unit increase in bone length were calculated from the slope of the linear regression relation between the load and acquired length. Because of the viscoelastic nature of the soft tissues, this increment rate will depend on the rate and the frequency of lengthening. The average increment rate of the load per unit length gain, and the average limit of the linear phase were compared between the patients with quasi continuous lengthening and those with step lengthening for both etiologies.

Data from the two groups were compared using Mann–Whitney U test. Correlation coefficients between the tensile force and acquired length in each patient were calculated with Pearson's test. A difference was considered significant when p values were less than 0.05.

3. Results

A loading test performed to evaluate accuracy of the measurement disclosed that the linearity was 5% with a hysteresis of 7%.

The average length gain in quasi-continuous femoral lengthening was 71 mm with a range of 35–92 mm, and that in stepwise femoral lengthening was 79 mm with a range 45–95 mm. No statistical difference of the length gain was noted between these groups. The average length gain in quasi-continuous tibial lengthening in achondroplastic patients was 95 mm with a range of 73–115 mm, and that in stepwise lengthening was 108 mm with a range of 82–132 mm. No significant difference of the length gain was noted either between these groups.

In all patients lengthening was uneventful, and the devices normally operated without occurrence of either disconnection or abnormal movement. There was

neither premature consolidation nor non-union of the distracted zone. No neurological disturbance was found during lengthening.

The circadian change of the tensile force in the patients undergoing quasi-continuous lengthening was markedly different from that in those receiving step lengthening. In the step-lengthening group, an acute increase in tensile force took place simultaneously with each step of lengthening and the time–course curve of the force resembled the stress–relaxation curve for a viscoelastic material. Fig. 2 shows the circadian change of the tensile force in stepwise femoral lengthening in a 25-year-old male. The vertical axis gives the tensile force data and the horizontal axis shows time. An acute increase of the tensile force was seen just after each 12-h step of 0.5 mm lengthening. The force then gradually decreased as time elapsed until the next step. An acute elevation of the load up to more than 550 N occurred at around 8 a.m. with lengthening of 0.5 mm. Then the force gradually decreased again and returned to almost the same level (about 480 N) as that seen just before distraction. In contrast, very little change of the baseline tensile force was noted in the patients undergoing quasi-continuous lengthening. The baseline level stayed at almost the same throughout the 24-h period. Fig. 3 shows a 17-year-old male undergoing quasi-continuous femoral lengthening. The force stayed at around the level of 330 N throughout 12-h period. The time course of the change in the force thus clearly differed from that for step lengthening. With the recording using a chart recorder, it was recognized that the tensile force made acute increases or decreases instantaneously synchronized with movements of the adjacent joints as is illustrated in Figs. 2 and 3.

In the initial stage of lengthening, the tensile forces increased almost linearly with the increase in bone length and the correlation between load and acquired length was very strong ($r = 0.95–0.99$, mean: 0.97). Fig. 4 shows auto-continuous femoral lengthening in a 15-year-old male with post traumatic growth retardation. The obvious diurnal change with day time increase and night time decrease was recognized, but the baseline tensile force increased linearly with increase in acquired length. But there was a limit of this linear increase. From this limit onwards, recurrent increases and decreases of the force occurred in turn, with baseline tensile force gradually increasing until the end of lengthening.

Fig. 5 shows the data of quasi-continuous tibial lengthening in a 29-year-old patient with achondroplasia. The vertical axis on the left indicates tensile force in unit of N and that on the right shows length gain in unit of mm. The horizontal axis indicates the date of

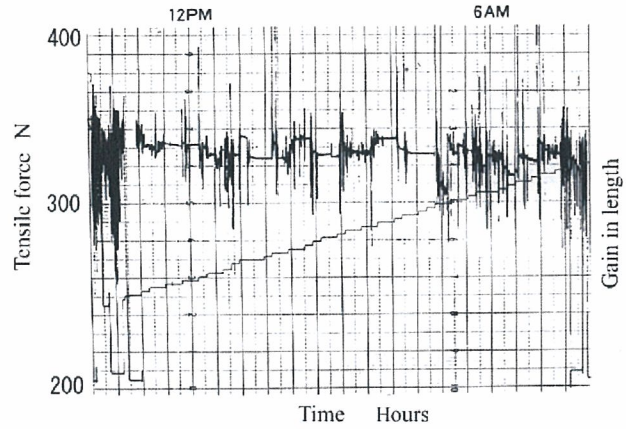

Fig. 3. The circadian change of the tensile force of a 17-year-old male undergoing auto-continuous femoral lengthening. The force stayed at around the level of 330 N throughout 12-h period.

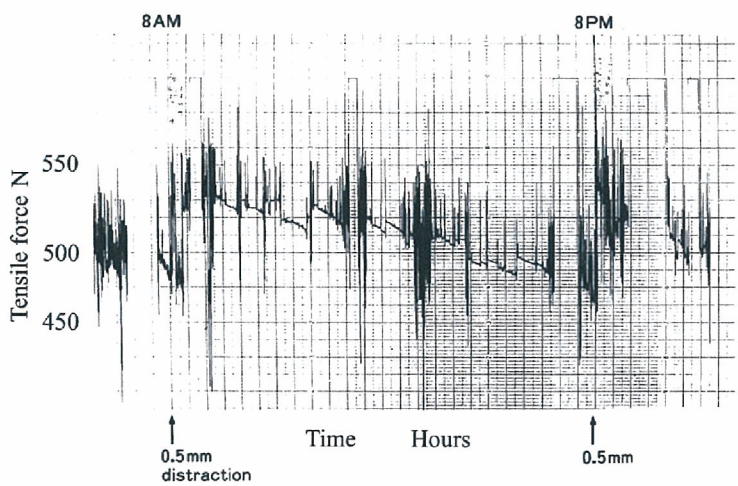

Fig. 2. The circadian change of the tensile force in stepwise femoral lengthening in a 25-year-old male. The vertical axis gives the tensile force data and the horizontal axis shows time. An acute increase of the tensile force was seen just after each 12-h step of 0.5 mm lengthening. The force then gradually decreased as time elapsed until the next step.

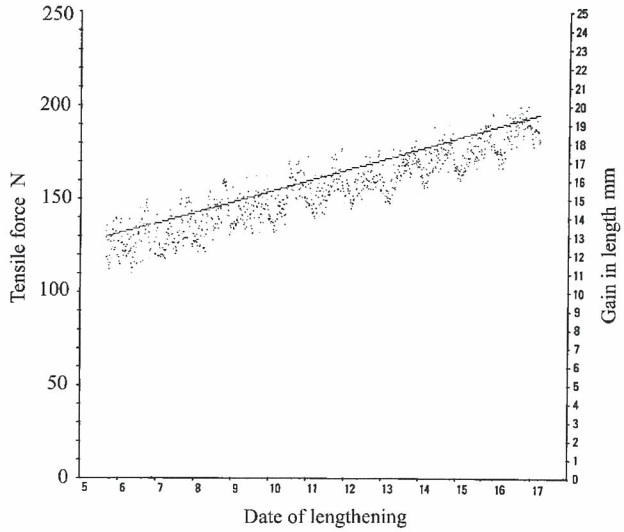

Fig. 4. The daily course of the tensile force in auto-continuous femoral lengthening of a 15-year-old male with post traumatic growth retardation. The obvious diurnal change with day time increase and night time decrease was recognized, but the baseline tensile force increased linearly with increase in acquired length.

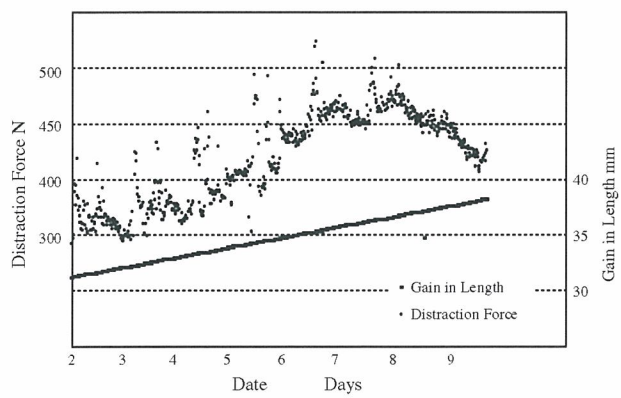

Fig. 5. The record of the tensile force of quasi-continuous tibial lengthening in a 29-year-old patient with achondroplasia. The vertical axis on the left indicates tensile force and that on the right shows length gain. The horizontal axis indicates the date of lengthening. On December 7, the load suddenly began to decrease. The force level of the left leg went down, although the lengthening speed (straight line) was not changed in this time period.

lengthening. On the 32nd day of lengthening (December 7), the load suddenly began to decrease. The force level of the left leg went down from around 450 to 400 N, although the lengthening speed (straight line) was not changed in this time period. Fig. 6 shows the time course of the load in this decrease phase. The horizontal axis indicates time in hours. This graph shows that the gradual decrease in the tensile force continued throughout 24-h period. Another decrease phase occurred on the 51st day (December 26), when the level went down from around 500 to 370 N (Fig. 7). This time, as the time–

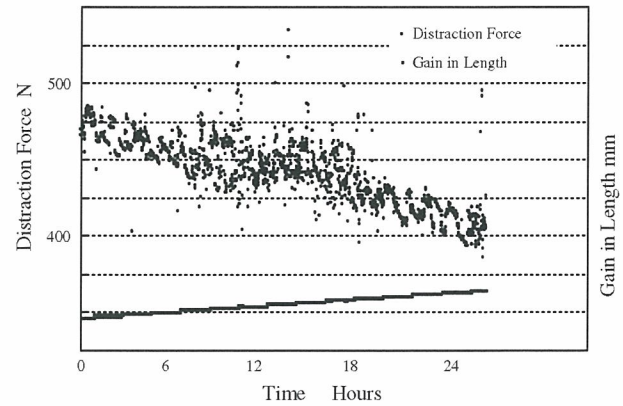

Fig. 6. The time course of the load in the decrease phase shown on the Fig. 5. The horizontal axis indicates time in hours. The gradual decrease in the tensile force continued throughout 24-h period.

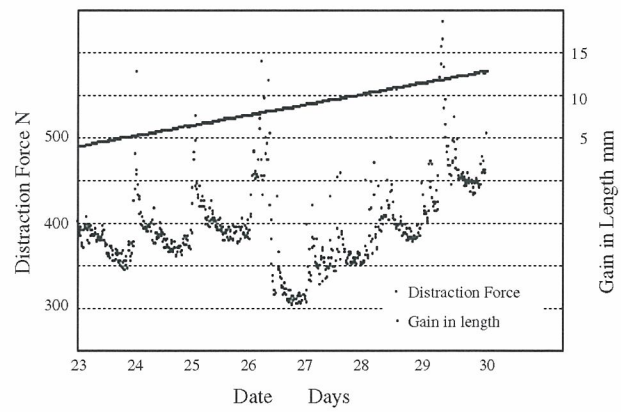

Fig. 7. Another decrease phase occurred on December 26, when the force level went down from around 500–370 N. This time, the process was more rapid.

course curve shows, the process occurred much more rapidly than before and more than 100 N was lost in 2 h (Fig. 8).

The average increment rate for quasi-continuous femoral lengthening at 0.7 μm/min (1.0 mm/day) was 8.9 N/mm with a standard deviation of 1.3 N/mm, while that for step femoral lengthening with the same rate was 9.4 N/mm with a standard deviation of 1.5 N/mm. There was no significant difference between the two. The rate was 9.7 N/mm with a standard deviation of 2.1 N/mm for quasi-continuous tibial lengthening in achondroplastic patients, and that for stepwise tibial lengthening was 10.1 N/mm with a standard deviation of 2.4 N/mm. There was no significant difference between the two either. Therefore, the lengthening frequency did not affect the load increment rate.

The average limit of the linear increase in force was 8.2% with a standard deviation of 1.9% of the original length in patients undergoing quasi-continuous femoral lengthening and 7.9% with a standard deviation of 2.1%

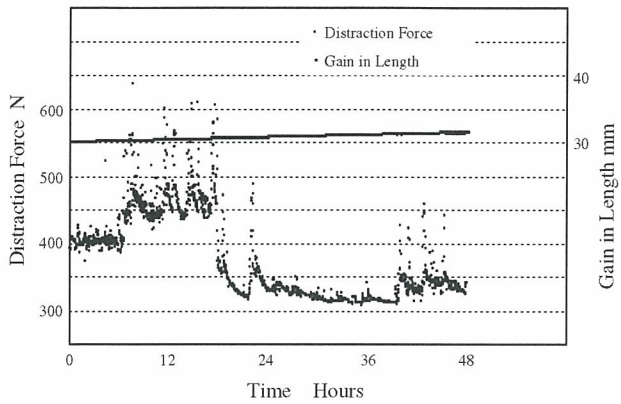

Fig. 8. The time–course curve of the process shown on the Fig. 7. The process was shown to occur much more rapidly than the process on the Fig. 5, and more than 100 N was lost in 2 h.

in stepwise femoral lengthening. There was no significant difference between the two groups. Likewise, the limit was 7.4% with a standard deviation of 1.8% for those having quasi-continuous tibial lengthening in achondroplastic patients and 7.0% with a standard deviation of 1.5% for those with stepwise tibial lengthening. There was no significant difference between the two groups. The lengthening frequency did not affect the range of the linear phase either.

4. Discussion

The Hifixator used in the current investigation was equipped with a load sensor attached to one of the pin clamps. The axial compressive forces applied to the bone fragments are transferred to the pin clamp by the fixation pins. The pin clamp has a bearing mechanism at the shaft–clamp interface, which allows smoothly sliding excursion along the shaft. Using this sliding pin clamp and the load sensor, the force applied to the bone fragments could be measured with linearity of 5%. A loading test of the fixator disclosed that there was sufficient linearity between the applied and measured loads. The first report that investigated tensile forces during bone lengthening was made by Leong et al. (1979), and since then, several reports were made on the process of the tensile forces. But previous studies have not clarified the accuracy of the measurement techniques they adopted.

The origin of the reaction force generated during bone lengthening is still controversial. Aronson et al. and Younger et al. reported that it originates mainly from distracted callus, because in case of premature consolidation, it rose high, and in case of non-union it stayed at a low level (Aronson and Harp, 1994; Younger et al., 1994). On the contrary, Simpson et al. speculated that the force developed mainly from tensioned soft tissues, because in patients with congenitally short limbs, they developed higher peak forces at each lengthening step followed by larger amount of force relaxation after a lengthening step compared to those of the patients with acquired or post-traumatic shortening (Simpson et al., 1996). Matsushita et al. also observed diurnal variation of the axial load generated during lengthening (Matsushita et al., 1999). This phenomenon also supported that the force was originated from soft tissues under tension. In fact, the force should originate from both callus and soft tissues, but the rate of contribution of each tissue to the overall distraction force have not been clarified yet. In addition, a technique to separately measure each of the forces either from callus or soft tissues has not been available until now. We also observed the diurnal variation of the load with the quasi-continuous lengthening.

The rate and frequency of limb lengthening have been decided mainly by evaluation of the amount of callus formation, without taking the condition of the soft tissues into consideration. Most orthopedic surgeons paid little attention to the soft tissues during bone lengthening, until severe joint contractures developed in some patients. They did not take the condition of the soft tissues into consideration to set the amount of the lengthening rate. Monitoring of the tensile force created by lengthening is advisable to prevent complications due to an excessive increase in soft tissue tension, such as joint contractures, the generation of angular deformities (Price and Cole, 1990), and damage to the articular cartilage of adjacent joints (Olney and Jayaraman, 1994). Simpson et al. and von Roemond et al. also referred to the complications due to the excessive increase of the tensile force (Simpson et al., 1996; van Roemund et al., 1992). Considering that severe equinus deformity of the ankle joint and flexion contracture of the knee joint can occur from a relatively earlier stage after tibial lengthening and cause severe disturbance of gait, the rate of lengthening should probably be slower than has previously been advocated. In cases without possibility of premature consolidation with too active callus formation, we had better adopt slower lengthening rate than has been previously recommended.

The circadian changes of the tensile force during quasi-continuous lengthening were very slight which could reduce the chance of inducing overstretching of the soft tissues when compared to the standard step lengthening with its acute increase of the force just after each step. In fact, the patients undergoing quasi-continuous lengthening seldom complained of pain associated with the lengthening procedure. This is considered to be due to differences in the time course of the tensile force between the auto-continuous and step lengthening procedures. But even with quasi-continuous lengthening, the tensile force steadily increased in its linear phase. This linear increase of the tensile force was also observed during

four times step lengthening as reported by Wolfson et al. (1990). The average increment of the load per unit length gain in quasi-continuous lengthening was not different from that of step lengthening. This means that frequency of the lengthening per day did not affect the amount of stiffness of the lengthened limb. In viscoelastic materials, load rate theoretically affects the material stiffness. But in this clinical study, we could not show that the quasi-continuous lengthening could reduce stiffness of the lengthened limb by greatly increasing the frequency of lengthening.

The sudden decrease in the load which appeared after the linear phase of increase was relatively rapid and more than 100 N of the load was lost in just a few hours. This relatively rapid relaxation may have been due to a rapid increase in the axial length of the soft tissues. However, the mechanism by which this process occurs appears to be entirely different from that involved in the initial stage of lengthening. The structural changes in the soft tissues at this stage might occur by some process other than axial growth or simple elastic stretch. Micro-rupture or some similar rapid process of structural change might be responsible for this event, but histological observation by an animal experiment will be necessary to give a correct explanation.

Controlling the rate of lengthening in order to suppress excessive elevation of the tensile force may be important to prevent the various complications mentioned above, but a certain level of tension may also be necessary to enhance tissue formation. Quantitative analysis to determine the optimum level of tension will require the study of many patients and much more data is needed before we can determine how much tension is appropriate and what level is harmful during limb lengthening. Analysis of the data obtained by the continuous monitoring of tensile force during lengthening may contribute to the avoidance of complications in the future.

Acknowledgement

This study was supported in part by the grant from the Society of Life Support Technology of Japan.

References

Aronson, J., Harp, J.H., 1994. Mechanical forces as predictors of healing during tibial lengthening by distraction osteogenesis. Clin. Orthop. Relat. Res. 301, 73–79.

Galardi, G., Comi, G., Lozza, L, Marchettini, P., Novarina, M., Facchini, R., Paronzini, A., 1990. Peripheral nerve damage during limb lengthening. J. Bone Joint Surg. 72 (1), 121–124.

Hiroshima, K., 1992. Changes of the hip joint following femoral lengthening. Orthopaedic Surgery and Traumatology 35 (1), 15–21 (in Japanese).

Leong, J.C.Y., Ma, R.Y.P., Clark, J.A., Cornish, L.S., Yau, A.M.M.C., 1979. Viscoelastic behavior of tissue in leg lengthening by distraction. Clin. Orthop. Relat. Res. 139, 102–109.

Matsushita, T., Nakamura, K., Kurokawa, T., 1999. Tensile force in limb lengthening: histogenesis or only mechanical elongation. Orthopedics (Thorofare, NJ) 22 (1), 61–63.

Ohnishi, I., Nakamura, K., Okazaki, H., Sato, W., Kurokawa, T., 2002. Evaluation of the fracture site mechanical properties in vivo by monitoring the motion of a dynamic pin clamp during simulated walking. Clin. Biomech. 17 (9–10), 687–697, November.

Olney, B.W., Jayaraman, G., 1994. Joint reaction forces during femoral lengthening. Clin. Orthop. Relat. Res. 301, 64–67.

Price, C.T., Cole, J.D., 1990. Limb lengthening by callotasis for children and adolescents. Clin. Orthop. Relat. Res. 250 (Jan.), 105–111.

Simpson, A.H., Cunningham, J.L., Kenwright, J., 1996. The forces which develop in the tissues during leg lengthening. A clinical study. J. Bone Joint Surg. 78 (6), 979–983.

van Roemund, P.M., Wijlens, R.A., Renooij, W., 1992. Continuous monitoring of forces during tibial lengthening by distraction epiphysiolysis. Acta Orthop. Belg. 58 (1), 63–68.

Wolfson, N., Hearn, T.C., Thomason, J.J., Armstrong, P.F., 1990. Force and stiffness changes during Ilizarov leg lengthening. Clin. Orthop. Relat. Res. 250, 58–60.

Younger, A.S., Mackenzie, W.G., Morrison, J.B., 1994. Femoral forces during limb lengthening in children. Clin. Orthop. Relat. Res. 301, 55–63.